Accepted Manuscript

Title: Novel mesoporous TiO$_2$(B) whisker-supported sulfated solid superacid with unique acid characteristics and catalytic performances

Authors: Licheng Li, Haiqin Yue, Tuo Ji, Wei Li, Xuejuan Zhao, Lei Wang, Jie She, Xiaoli Gu, Xiaobao Li

Please cite this article as: Licheng L, Yue H, Tuo J, Wei L, Xuejuan Z, Lei W, Jie S, Xiaoli G, Xiaobao L, Novel mesoporous TiO$_2$(B) whisker-supported sulfated solid superacid with unique acid characteristics and catalytic performances, *Applied Catalysis A, General* (2019), https://doi.org/10.1016/j.apcata.2019.01.025

Novel mesoporous TiO$_2$(B) whisker-supported sulfated solid superacid with unique acid characteristics and catalytic performances

Licheng Li [a,e*], Haiqin Yue [a], Tuo Ji [b], Wei Li [c,e], Xuejuan Zhao [d], Lei Wang [a,f], Jie She [a], Xiaoli Gu [a], Xiaobao Li [a]

[a] College of chemical engineering, Nanjing Forestry University, 210037, Jiangsu, China.

[b] Department of chemical and biomolecular engineering, The university of Akron, 44325, Akron, OH, United states.

[c] European Bioenergy Research Institute and Aston Institute of Materials Research, Aston University, Birmingham, B4 7ET, United Kingdom.

[d] School of Materials Engineering, Nanjing Institute of Technology, 211167, Jiangsu, China

[e] State Key Laboratory of Materials‑Oriented Chemical Engineering, Nanjing Tech University, 210009, Jiangsu, China

[f] CNOOC Changzhou Paint and Coatings Industry Research Institute Co., Ltd., 213016, Jiangsu, China

Graphical abstract
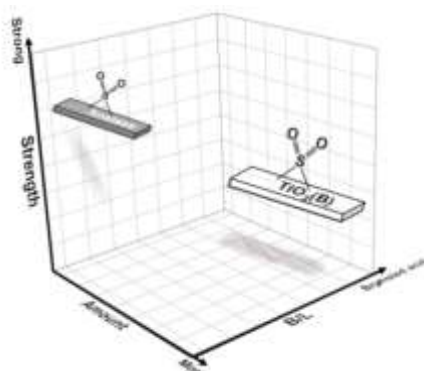
Highlights

➢ A novel sulfated solid superacid is synthesized firstly using mesoporous TiO$_2$(B) whisker as the support.

➢ Sulfated TiO$_2$(B) has more total acid amount, higher percentage of Brønsted acid and weaker acid strength than that of sulfated anatase under similar sulfate group amount.

➢ Sulfated TiO$_2$(B) shows increased esterification reaction rate and decreased alkylation byproduct selectivity compared with that of SO$_4^{2-}$/Anatase.

➢ The unique structure-performance relationship of sulfated TiO$_2$(B) may open a strategy to mediate the acid characteristic for sulfated solid superacid.

Abstract: Mesoporous TiO$_2$(B) whisker was firstly applied as a support for synthesizing the novel sulfated solid superacid (SO$_4^{2-}$/TiO$_2$(B)). According to NH$_3$-TPD, TG and Py-IR characterization results, it was found that the similar amount of sulfate group on TiO$_2$(B) and anatase showed significantly different acid characteristics and catalytic performances. The total acid amount of SO$_4^{2-}$/TiO$_2$(B) was about 1.8 times as anatase-supported sulfated solid superacid (SO$_4^{2-}$/Anatase). Simultaneously, the SO$_4^{2-}$/TiO$_2$(B) possessed higher percentage of Brønsted acid and more weak-medium acid strength than

SO_4^{2-}/Anatase. These acidic properties endowed SO_4^{2-}/TiO_2(B) with the increased esterification reaction rate and decreased alkylation byproduct selectivity compared with that of SO_4^{2-}/Anatase. Structure-performance analysis exhibited that there were more bridged bidentate sulfate groups coordinated to the TiO_2(B) in SO_4^{2-}/TiO_2(B), which could induce more Ti cations than that of the chelating one. This was the key factor to be responsible for the unique acid characteristics of SO_4^{2-}/TiO_2(B). The present work provides a novel solid superacid and might open a strategy to mediate the acid characteristic for sulfated solid superacid.

Keywords: TiO_2(B); sulfated solid superacid; acid properties; coordination; catalysis

Introduction

Sulfated solid superacid (SO_4^{2-}/M_xO_y), distinguished from conventional liquid acids, has significant advantages of high catalytic-activity, rapid separation, easy recycling and low corrosivity. Since Hino and Arata firstly found the superacidic characteristics of SO_4^{2-}/M_xO_y [1], this type of materials has been attracting numerous attentions of various fields. Towards dissimilar requirements of hundreds of acid-catalyzed reactions, it is of great scientific and industrial significance to design and achieve the specified sulfated solid superacid [2-6]. Owing to the simple composition (i.e. sulfate group and support), most efforts for developing novel SO_4^{2-}/M_xO_y are mainly focused on choice or synthesis of the supports [6, 7].

The improvements in geometrical factors of support were preliminarily considered for mediating the acid properties of solid superacid and simultaneously endowing them with some new physical functions. For instance, enlarging surface area of support could increase the adsorption amount of acidic precursors, which benefited the formation of more number of acid sites in corresponding solid superacid

[8-10]. Moreover, constructing mesoporous framework of support can effectively promote the mass transfer of reactants and resultants [11-14]. Besides these, to accelerate the separation from react system, the supports of SO_4^{2-}/M_xO_y are usually synthesized into the one with special morphologies, such as hierarchical, layered and linear structure [15-17]. Apparently, the adjustment of geometrical factors of support mainly influences the macroscopic parameters of solid superacid.

On the other hand, the individual structure of acid site of SO_4^{2-}/M_xO_y is distinctly different on various supports. For example, sulfate groups loaded on ZrO_2, TiO_2 and Fe_2O_3 could obtain the solid superacids with the Hammett value (H_o) range from 13.0 to 16.1, suggesting the presence of hundreds or thousands of times acid strength difference between them [2, 3, 5]. Moreover, numerous efforts are devoted into incorporation of structural promoter or combination of several supports for synthesizing the solid superacid with specific acid type, acid amounts and acid strength [2, 6, 18]. Essentially, these approaches change the electronegativity and coordination of superficial atoms of supports to affect their structure of acid sites. Both are two key factors to influence the electronic induction of sulfate groups with supports, which could determine superacidic characteristics of SO_4^{2-}/M_xO_y [2, 3, 19, 20]. To date, only a few metal oxides (M_xO_y), e.g. ZrO_2, TiO_2, Fe_2O_3, SnO_2, etc., are found to be qualified for the support of SO_4^{2-}/M_xO_y. That means SO_4^{2-}/M_xO_y must contain one of above-mentioned metal oxides.

In comparison, even on single metal oxides, their various crystal phases or exposed facets can significantly influence the acid properties of corresponding solid superacids. Tetragonal ZrO_2-supported sulfated solid superacid usually displayed several times the catalytic activity as monoclinic ZrO_2-supported sulfated solid superacid. This is mainly attributed to the better suitable surface arrangement of tetragonal ZrO_2 with sulfate group for obtaining the superacidity [21-23]. TiO_2, another

support for SO_4^{2-}/M_xO_y, has three common crystal phases, anatase, rutile and brookite. It was found that the concentration of surface acid sites per unit area was relatively higher in anatase TiO_2 than that in rutile one [24]. Moreover, the sulfate groups in brookite TiO_2 were less deformed and consequently showed more stable than those in anatase [25]. Besides three crystal phases, $TiO_2(B)$ is the other one metastable phase of TiO_2, firstly synthesized by Marchand et al. in 1980 [26]. Due to its more exotic layered structure, $TiO_2(B)$ has attracted attention as prospective lithium electrode, sensor material, and photocatalyst [27-30]. Specially, there are two, three or four-coordinated oxygen atom existed in the surface of $TiO_2(B)$, while there is only one form of four-coordinated oxygen atom in three common TiO_2 polymorphs [31-33]. As mentioned above, the special coordination of superficial atoms of $TiO_2(B)$ would result in the formation of different acid properties of corresponding solid superacids and possess varying catalytic performances.

In the present work, for the first time, a mesoporous $TiO_2(B)$ whisker was applied as the support to prepare a novel sulfated solid superacid ($SO_4^{2-}/TiO_2(B)$). Indeed, the obtained $SO_4^{2-}/TiO_2(B)$ could exhibit significantly different acidic characteristics compared with that of sulfate groups on anatase TiO_2. Simultaneously, the $SO_4^{2-}/TiO_2(B)$ possessed excellent esterification catalytic performance and low selectivity of alkylation byproduct. Furthermore, the whisker morphology of $TiO_2(B)$ could facilitate the rapid separation of $SO_4^{2-}/TiO_2(B)$. In the following context, the physicochemical properties of as-prepared samples were systematically studied by Raman, SEM, HRTEM, BET, NH_3-TPD, Py-IR, and so on. The necessary data for structure-performance relationship analyses were provided by TG, FT-IR and XPS.

Experimental

Preparation of mesoporous $SO_4^{2-}/TiO_2(B)$

The preparation process of mesoporous $SO_4^{2-}/TiO_2(B)$ contains two main steps, synthesis of mesoporous $TiO_2(B)$ and loading of acid sites. The mesoporous $TiO_2(B)$ is prepared from potassium titanate, which has been reported in our previous work [34, 35]. Briefly, the raw material K_2CO_3 and $TiO_2 \cdot nH_2O$ were mixed at a Ti/K molar ratio of 0.95 for 12 h. After being dried, mixture was calcined at 860 °C for 4 h to obtain the potassium titanate. Subsequently, the calcined mixture was separately placed into an autoclave filled with $CaCl_2$ saturated solution and being heated at 180 °C for 24 h. The obtained powders were further ion-exchanged to remove the potassium ion and then was calcined at 500 °C for 2 h to acquire the mesoporous $TiO_2(B)$. The acidification process of $TiO_2(B)$ was carried out by a conventional impregnation method using liquid H_2SO_4 as acid source. The $TiO_2(B)$ powders were immersed into excessive H_2SO_4 aqueous solution (1 M) with stirring for overnight. After the solution was filtered, the collected powders were dried and calcined at 450 °C for 2 h to obtain the $SO_4^{2-}/TiO_2(B)$ solid superacid.

In addition, a commercial anatase TiO_2 (AR, Jingrui New Material Co., Ltd, China) was used as a support for preparing the control sample. The acidification process was consistent with above-mentioned method, and the achieved solid superacid was denoted as $SO_4^{2-}/Anatase$.

Characterization

Raman spectra were recorded on a Horiba HR 800 spectrometer equipped with a CCD camera detector. The wavelength of excitation light was 514 nm and the signals were sampled in the range from 100 cm^{-1} to 1100 cm^{-1}. Nitrogen adsorption/desorption at 77 K was carried out on a Micromeritics ASAP 2020 system. The surface area of samples was calculated by BET method and pore volume was obtained by nitrogen adsorption with P/P_0 of 0.99. Pore size distribution was determined from adsorption isotherms using Barrett-Joyner-Halenda method. Fourier

transform infrared spectroscopy (FT-IR) was performed on a Nicolet 6700 spectrometer in the wavenumber range from 2000 cm^{-1} to 400 cm^{-1} with a resolution of 4 cm^{-1}. The morphology of the samples was studied by Scanning electron microscopy (SEM, JEM-7600F). Furthermore, the nanoscale morphology of samples was collected by Transmission electron microscope (TEM, JEM-2010). Thermo-gravimetric (TG) analysis was carried out on a Model SDT 2960 (TA, America) instrument. The experiment was conducted under nitrogen atmosphere and the test temperature was started from 40 ^{o}C to 950 ^{o}C at a heating rate of 10 ^{o}C·min^{-1}. X-ray photoelectron spectroscopy (XPS, ESCALAB 250) equipped with a monochromatic Al Kα X-ray beam was used to analyze the chemical state of Ti and S on the solid surface. All binding energies of samples were referenced to the C1s peak (284.6 eV), which arose from the adventitious hydrocarbons. NH_3 temperature programmed desorption (NH_3-TPD) experiment was conducted on a TP-5000 equipment (Tianjin Xianquan Co., Ltd., China). Initially, the samples were in-situ pretreated in He at 300 ^{o}C for 1 h. Subsequently, the samples were cooled down to room temperature followed by injecting 5% NH_3/He gas till saturation of adsorption capacity. After being switched to pure He purge at a flow rate of 30 mL·min^{-1} for about half an hour, the NH_3-TPD signal of sample was recorded as a function of temperature from 40 ^{o}C to 580 ^{o}C at a heating rate of 5 ^{o}C·min^{-1}. Pyridine absorption infrared (Py-IR) measurements were also performed on the Nicolet 6700 spectrometer device equipped with a diffuse reflectance attachment and an MCT detector. The tested powders were placed into an in-situ chamber and smoothed. Initially, the powders were pretreated with He (30 mL·min^{-1}) at 300 ^{o}C for 1 h, cool down to room temperature and scanned for the background. Thereafter, gaseous pyridine was adsorbed on powders until the adsorption saturation. He was injected into the

in-situ chamber and purged the powders for 1 h. Finally, the infrared spectrum in the region from 1700 cm^{-1} to 1400 cm^{-1} could be recorded.

Catalyst activity evaluation

Esterification reaction of acetic acid and n-butanol was employed to evaluate the catalytic performance of various solid superacids. The reaction was carried out in a 100 mL of three-necked flask equipped with a reflux condenser, which was controllably heated in an oil bath. Originally, 10 mL of acetic acid and 15 mL of n-butanol were added into the three-necked flask. 0.5 g of solid superacid was added once the temperature of liquid reactants reached up to 103±1 ^{o}C. After 45 min of continuous reaction, the liquid products were collected and their components were identified using a GC-9890B gas chromatograph equipped with a 30 m OV-101 capillary column and a FID detector. The recycle experiment was carried out by collecting solid superacid back to three-necked flask. The corresponding stoichiometric amount of reactants, reaction condition and product analyses were consistent with those of above-mentioned esterification process.

Alkylation reaction of benzyl alcohol and anisole was also conducted in the above experimental apparatus. The molar ratio of anisole to benzyl alcohol was 9.6 and the usage amount of solid superacid was 0.2 g·mL^{-1} based on the volume of benzyl alcohol. After continuous reaction at 130 ^{o}C for 45 min, the liquid product was collected by filtering the solid superacid. The component information of liquid product was identified by above GC-9890B gas chromatography using naphthalene as internal standard substance.

Results and discussion

Structural information. The crystal information of solid superacids was analyzed by Raman spectrum. As shown in Fig. 1, the obvious peaks at 119 cm^{-1}, 196 cm^{-1}, 238 cm^{-1}, 251 cm^{-1}, 364 cm^{-1}, 405 cm^{-1}, 433 cm^{-1}, 467 cm^{-1}, 632 cm^{-1} and 660 cm^{-1} are indexed to the TiO$_2$(B) phase.

Additionally, SO_4^{2-}/Anatase exhibited Raman bands at 139 cm^{-1}, 393 cm^{-1}, 513 cm^{-1} and 634 cm^{-1}, which are ascribed to the anatase phase [27, 30, 36]. Both results indicate the pure crystal phase in two respective supports of sulfated solid superacids.

(Fig. 1)

The morphology of SO_4^{2-}/TiO_2(B) and SO_4^{2-}/Anatase were characterized by SEM and TEM. Fig. 2(a & b) shows that the SO_4^{2-}/TiO_2(B) has a uniform whisker-like morphology, while the SO_4^{2-}/Anatase appears to be irregular ellipsoidal particles. TEM images (as seen in Fig. 2(c & d)) further reveal the individual morphology of SO_4^{2-}/TiO_2(B) and SO_4^{2-}/Anatase. The width and length of SO_4^{2-}/TiO_2(B) whiskers are dozens of nanometers and hundreds of nanometers, respectively. SO_4^{2-}/Anatase exhibits the particle size of dozens of nanometers. In high resolution TEM images (as seen in Fig. 2(e)), the SO_4^{2-}/TiO_2(B) has lattice fringes with a d-spacing of 0.30 nm and 0.35 nm, which is in accordance with (-401) and (110) planes of TiO_2(B), respectively. Fig. 2(f) displays the lattice fringes with a d-spacing of 0.23 nm and 0.35 nm assign to the (004) and (101) lattice planes of anatase phase. These demonstrate the presence of TiO_2(B) phase and anatase phase in SO_4^{2-}/TiO_2(B) and SO_4^{2-}/Anatase, respectively, as consistent with the results of above Raman spectra.

(Fig. 2)

Fig. 3 displays the nitrogen adsorption-desorption isotherms of SO_4^{2-}/TiO_2(B) and SO_4^{2-}/Anatase. Both samples exhibit a type IV isotherm characteristic, suggesting the presence of mesoporous structure in SO_4^{2-}/TiO_2(B) and SO_4^{2-}/Anatase. Moreover, the type H3

hysteresis loop of $SO_4^{2-}/TiO_2(B)$ corresponds to irregular porous structure [37, 38], which is related to the layered structure of $TiO_2(B)$ precursor. After high-temperature calcination, the asymmetric rearrangement or superimposition of $TiO_2(B)$ precursor leads to formation of specific crystal structure and slit pore of titania [35]. Table 1 shows that the surface area (S_{BET}) of $SO_4^{2-}/TiO_2(B)$ is 78.8 $m^2 \cdot g^{-1}$, slightly higher than 63.1 $m^2 \cdot g^{-1}$ of $SO_4^{2-}/Anatase$. Instead, $SO_4^{2-}/TiO_2(B)$ has an obviously lower pore volume (V_p) than $SO_4^{2-}/Anatase$ does (0.10 $cm^3 \cdot g^{-1}$ versus 0.24 $cm^3 \cdot g^{-1}$). The low pore volume of $SO_4^{2-}/TiO_2(B)$ suggests the close distance between two sides of slit pore, as also proved by the relatively small pore size distribution of $SO_4^{2-}/TiO_2(B)$ (inset picture of Fig. 3).

(Fig. 3)

(Table 1)

Acidic properties. The acid strength distribution and acid amount of solid superacids were characterized by NH_3-TPD. All the NH_3-TPD curves can be divided into three temperature regions of below 200 °C, 200 °C~450 °C and above 450 °C, which are ascribed to the adsorption of NH_3 onto weak acid sites, that onto medium acid sites and that onto strong acid sites, respectively. As depicted in Fig. 4, two broadened NH_3 desorption peaks at 125 °C and 508 °C can be observed in $SO_4^{2-}/Anatase$, which indicate that its content of weak acid and strong acid are relatively more than that of medium acid. The present NH_3-TPD pattern of $SO_4^{2-}/Anatase$ is almost same as the literatures' results [8, 9, 39, 40]. Nevertheless, the $SO_4^{2-}/TiO_2(B)$ shows remarkably different acid strength distribution from $SO_4^{2-}/Anatase$ does. NH_3 molecules on $SO_4^{2-}/TiO_2(B)$ are mainly desorbed at the temperature region of 200

°C~450 °C, which demonstrates the leading part of medium acid sites in $SO_4^{2-}/TiO_2(B)$. The amount of various acid sites in $SO_4^{2-}/TiO_2(B)$ and $SO_4^{2-}/Anatase$ are quantitatively calculated and the results are summarized in Table 1. It reveals that the total acid amount of $SO_4^{2-}/TiO_2(B)$ is about 1.8 times as that of $SO_4^{2-}/Anatase$. Moreover, 70% of the total acid amount (N_{Total}) of $SO_4^{2-}/TiO_2(B)$ are attributed to the contribution of medium acid, whereas the strong acid amount (N_{Strong}) of $SO_4^{2-}/TiO_2(B)$ is less than that of $SO_4^{2-}/Anatase$ (6.6 $\mu mol \cdot g^{-1}$ versus 8.3 $\mu mol \cdot g^{-1}$). According to these results, it can be confirmed that the $SO_4^{2-}/TiO_2(B)$ has more acid amount but relatively weak acid strength compared with the $SO_4^{2-}/Anatase$ does.

(Fig. 4)

The acid type of solid superacids was identified by infrared spectroscopic studies of adsorbed pyridine. As presented in Fig. 5, the obvious band located at 1606 cm^{-1} is attributed to the physical adsorption of pyridine with hydrogen bonding of surface hydroxyl group of solid superacids [41, 42]. Additionally, the band at 1540 cm^{-1} is assigned to the adsorption of pyridine onto Brønsted acid sites, and the band at 1490 cm^{-1} is assigned to the coordinative bound of pyridine to both Brønsted and Lewis acid sites. The rightmost obvious band at 1445 cm^{-1} is ascribed to the adsorption of pyridine onto Lewis acid sites [41, 42]. Generally, anatase phase and $TiO_2(B)$ phase merely have Lewis acid sites [32, 43]. Hence, the band at 1490 cm^{-1} in two supports (Anatase and $TiO_2(B)$) is completely attributed to the adsorption of pyridine onto Lewis acid sites. Compared with their bare supports, both $SO_4^{2-}/TiO_2(B)$ and $SO_4^{2-}/Anatase$ show a new band at 1540 cm^{-1} corresponding to Brønsted acid. Noteworthy, in the spectrum of $SO_4^{2-}/TiO_2(B)$, the intensity of the band at 1490 cm^{-1} is distinctly lower than that at 1445

cm^{-1}, which is opposite to that in SO_4^{2-}/Anatase and two supports. Based on above analyses, the band at 1490 cm^{-1} of SO_4^{2-}/TiO$_2$(B) and SO_4^{2-}/Anatase should contain contribution of the adsorption of pyridine onto Brønsted acid sites. It means that the relatively higher intensity of band at 1490 cm^{-1} can be attributed to the larger ratio of Brønsted acid sites in SO_4^{2-}/TiO$_2$(B), as also reflected by more observable band at 1540 cm^{-1} in SO_4^{2-}/TiO$_2$(B) spectrum. According to following equation (1 & 2) [44], the calculated results in Table 1 display that Brønsted acid takes up 70.9 mol% of the total acid amount in SO_4^{2-}/TiO$_2$(B), whereas 41.5 mol% in SO_4^{2-}/Anatase.

$$X_{Brønsted} = \frac{I_B}{I_B + 0.752I_L} \times 100\% \qquad (1)$$

$$X_{Lewis} = \frac{I_L}{1.329I_B + I_L} \times 100\% \qquad (2)$$

where I_B and I_L are the integrated area of peaks at 1540 cm^{-1} and 1445 cm^{-1}, respectively. X_{Lewis} and $X_{Brønsted}$ are the molar percentage of Lewis acid sites and Brønsted acid sites, respectively.

(Fig. 5)

Catalytic performance. Esterification of acetic acid with n-butanol and alkylation of anisole with benzyl alcohol were chosen as model reactions to evaluate the catalytic performance of various solid superacids. As exhibited in Table 2, the esterification reaction rate (r_E) of SO_4^{2-}/TiO$_2$(B) is 4.25 $mmol_{BuOH} \cdot g^{-1} \cdot min^{-1}$, which is higher than that of SO_4^{2-}/Anatase (2.87 $mmol_{BuOH} \cdot g^{-1} \cdot min^{-1}$). After excluding contribution of spontaneous reaction or supports (1.15 $mmol_{BuOH} \cdot g^{-1} \cdot min^{-1}$ and 0.95 $mmol_{BuOH} \cdot g^{-1} \cdot min^{-1}$ for TiO$_2$(B) and Anatase, respectively), the esterification catalytic performance of SO_4^{2-}/TiO$_2$(B) brought by acid sites shows about 60% of increase compared with that of SO_4^{2-}/Anatase. It is acknowledged that the improvement in reaction rate of conventional

acid-alcohol esterification is closely related to the increased acid amount, especially Brønsted acid amount [45-48]. Above NH_3-TPD and Py-IR analyses have shown that $SO_4^{2-}/TiO_2(B)$ possessed more total acid amount and relatively higher percentage of Brønsted acid than $SO_4^{2-}/Anatase$ did. This could be responsible for the excellent esterification performance of $SO_4^{2-}/TiO_2(B)$.

(Table 2)

However, the superiority in catalytic performance of $SO_4^{2-}/TiO_2(B)$ is not observed in alkylation reaction that $SO_4^{2-}/TiO_2(B)$ has a relatively lower reaction rate of benzyl alcohol (r_A) than $SO_4^{2-}/Anatase$ does (1.39 $mmol_{BA} \cdot g^{-1} \cdot min^{-1}$ versus 1.95 $mmol_{BA} \cdot g^{-1} \cdot min^{-1}$). Note that the activation of alkylation reactants requires to be carried out on strong acid sites [49-51]. As shown in Fig. 4 and Table 1, the strong acid amount of $SO_4^{2-}/TiO_2(B)$ is less than that of $SO_4^{2-}/Anatase$. Hence, the unsatisfactory alkylation reaction rate of $SO_4^{2-}/TiO_2(B)$ could be associated with the insufficient strong acid amount. Moreover, besides different reaction rates, the alkylation selectivities of $SO_4^{2-}/TiO_2(B)$ and $SO_4^{2-}/Anatase$ are also varied. There are three resultants, ortho-benzylanisole, para-benzylanisole and dibenzylether in the alkylation reaction of anisole with benzyl alcohol. Among them, ortho-benzylanisole and para-benzylanisole are the target products of alkylation reaction, while dibenzylether is the by-product [52, 53]. As shown in Table 2, the selectivity of dibenzylether ($S_{Dibenzylether}$) is 20.57% for $SO_4^{2-}/TiO_2(B)$, which is relatively lower than that of $SO_4^{2-}/Anatase$ (26.07%) under the same reaction condition. Domen et al. comparatively studied three solid acids with dibenzylether selectivity of 11%, 13% and 18%. They found the correlation of an increase in Brønsted acid sites with a decrease in dibenzylether selectivity [52]. It suggests that the

more Brønsted acid sites could alter alkylation reaction to generate less dibenzylether and more (ortho and para)-benzylanisole. Apparently, the present result of alkylation reaction is similar to Domen's work. As shown in Py-IR analyses in Fig. 5, $SO_4^{2-}/TiO_2(B)$ has a higher percentage of Brønsted acid sites than $SO_4^{2-}/Anatase$, which can account for its relatively low selectivity of byproduct dibenzylether.

(Fig. 6)

Herein, we introduce another advantage of $SO_4^{2-}/TiO_2(B)$ towards application that is the easy separation. Fig. 6 shows two solid superacids' solid-liquid separation state as a function of time. The $SO_4^{2-}/TiO_2(B)$ suspension is clarified only at 60 min, while the $SO_4^{2-}/Anatase$ one is still kept turbid after 90 min. SEM and TEM images in Fig. 2 have displayed that the $SO_4^{2-}/TiO_2(B)$ possessed a uniform whisker-like morphology, which could be beneficial to be precipitated and separated from liquid system compared with the ellipsoidal shape $SO_4^{2-}/Anatase$. The rapid precipitation of $SO_4^{2-}/TiO_2(B)$ proves the easy solid-liquid separation, which promotes their further application potentiality. On basis of this, the recycling performance of $SO_4^{2-}/TiO_2(B)$ and $SO_4^{2-}/Anatase$ are further comparatively studied. It can be observed that both of them have a certain degree of deactivation after several cycling. By comparison, $SO_4^{2-}/TiO_2(B)$ shows obviously lower decline in reaction rate than $SO_4^{2-}/Anatase$, which could be related to the less mass loss caused by easy separation of $SO_4^{2-}/TiO_2(B)$. The leach of sulfate groups away from solid superacid also cannot be excluded to influence their decrease in reaction rates [4, 9]. Anyhow, $SO_4^{2-}/TiO_2(B)$ could show significantly better stability than $SO_4^{2-}/Anatase$ in the present studies.

Structure-performance relationship. In above section, it has illuminated the correlation of acid properties of $SO_4^{2-}/TiO_2(B)$ and $SO_4^{2-}/Anatase$ with their catalytic performances. The following context is focused on analysis of the reason why $SO_4^{2-}/TiO_2(B)$ exhibits different acidic characteristics from that of $SO_4^{2-}/Anatase$.

The influence of physical morphology and structure of solid superacid on its acid properties is preliminarily analyzed. In Fig. 2, $SO_4^{2-}/TiO_2(B)$ has exhibited the whisker-like shape while $SO_4^{2-}/Anatase$ was appeared in granular. The morphological difference between them mainly influenced their separations from liquid system, as proved in Fig. 6. For the acid properties of solid superacids, it was generally considered to be more closely related to their surface area. The support with larger surface area could easily adsorb more acidic precursors to increase the sulfate group content and further form the more acid sites [8-11]. As shown in Table 1, $SO_4^{2-}/TiO_2(B)$ did have the relatively larger surface area than $SO_4^{2-}/Anatase$ (78.8 m^2 g^{-1} versus 63.1 m^2 g^{-1}). Accordingly, it is necessary to analyze the content of sulfate group in two solid superacids.

In many published literatures, the sulfate content of solid acid was determined by thermogravimetry technique [54-57]. The weight loss stage of solid superacid at above 550 °C is attributed to the volatilization of sulfate group in the form of SO_3, which can be used to calculate the sulfate group content [57]. As shown in Fig. 7, the weight loss at such temperature range of two samples are multiplied by a coefficient (1.2, i.e. relative molecular weight ratio of SO_4^{2-} to SO_3) to achieve their sulfate group contents ($W_{SO_4^{2-}}$). The corresponding results are listed in Table 1. The sulfate group content of $SO_4^{2-}/TiO_2(B)$ is 2.22 %, which is slightly higher (1.1 times) than that of $SO_4^{2-}/Anatase$ (1.97%). Indeed, the large surface area of $SO_4^{2-}/TiO_2(B)$ could increase its own sulfate group

content, which is in accordance with published results [8-10]. Nevertheless, as seen in Table 1, NH_3-TPD results show that SO_4^{2-}/TiO_2(B) possesses 1.8 times the total acid amount as that of SO_4^{2-}/Anatase. Obviously, such tiny difference in sulfate group content between SO_4^{2-}/TiO_2(B) and SO_4^{2-}/Anatase cannot account for their significant gap in acid amount (1.1 times versus 1.8 times). In terms of the acid amount per unit of sulfate group, the SO_4^{2-}/TiO_2(B) is almost 1.6 times as that of SO_4^{2-}/Anatase. Similarly, the sulfate group amount also cannot be responsible for the different percentage of Brønsted acid between SO_4^{2-}/TiO_2(B) and SO_4^{2-}/Anatase (70.9 % versus 41.5%, as seen in Table 1). These results indicate SO_4^{2-}/TiO_2(B) and SO_4^{2-}/Anatase have dissimilar structure of acid sites.

(Fig. 7)

FT-IR spectrum was employed to characterize the structure of sulfate groups. As displayed in Fig. 8, several bands in the region of 1300 cm^{-1}~900 cm^{-1} demonstrate the bidentate coordination of sulfate groups to Ti cations of support [9, 19, 58]. Among them, the bands at around 1300 cm^{-1}~1100 cm^{-1} are attributed to the stretching of S=O vibrations. The asymmetric stretching of S=O vibrations generally appear at relatively higher wavenumber (> 1200 cm^{-1}) and the symmetric one located in relatively lower wavenumber (< 1200 cm^{-1}). Moreover, the S-O stretching vibrations of the sulfate group are presented in the range from 1100 cm^{-1} to 900 cm^{-1}. Analogously, the wavenumber assigned to asymmetric stretching of S-O band approaches to lower wavenumber location (< 1000 cm^{-1}) and that to its symmetric stretching vibration shifts to a higher one (> 1000 cm^{-1}) [9, 19, 58]. Besides the appearance of these bands, it also can be seen a certain wavenumber shift of every IR peak corresponding to S-O or S=O bond vibration between

$SO_4^{2-}/TiO_2(B)$ and $SO_4^{2-}/Anatase$, which can further confirm their structure of sulfate groups are different.

(Fig. 8)

To date, there is not a definite structure model corresponding to the acid site of sulfated solid superacid [3, 5, 59]. It is summarized that there are two familiar types of bidentate sulfate group coordinated to TiO_2, namely chelating bidentate and bridged bidentate [5, 58-62], as shown in Fig. 9. In the configuration of chelating bidentate coordination (Fig. 9(a)), one sulfate group is chemically linked to one Ti cation, while one sulfate group to two Ti cations in the bridged bidentate coordination (Fig. 9(b)). In detail, the sulfate group is shaped in tetrahedral structure and its S-O bond length is about 0.15±0.2 nm [63]. The Ti-O bonds of titania surface have a length of 0.16 nm~0.24 nm [31]. HRTEM results in Fig. 2 have shown that the d-spacing between Ti atoms in $TiO_2(B)$ and anatase phase were in the range of 0.23 nm~0.35 nm [31]. Theoretically, both above configurations are feasible to be present in TiO_2-supported solid superacid by adjusting bond length and bond angle of related atoms.

(Fig. 9)

In electron induction theory, the electron of metal cations of support are induced to transfer to sulfate groups, which results in the strong electron withdrawing ability of metal cations to form Lewis acid sites. The Brønsted acid sites are generated by synergistic interaction of surface hydroxyl group or adsorbed water on metal oxides neighboring sulfate group with Lewis acid sites [2, 19, 42]. The electron-deficient metal cations of support which are chemically bonding to sulfate groups are the real acid sites. In the model structure of acid sites (as shown in Fig 9),

one bridged bidentate sulfate group attracts the electrons from two linked Ti cations while the chelating bidentate one only from one linked Ti cation. It illustrates that more Ti cations could be induced to form Lewis acid sites in the configuration of bridged bidentate coordination compared with that in chelating one under the same sulfate group amount. As a result, more Brønsted acid sites can also be generated in the configuration of bridged bidentate coordination. In Fig. 4 and Fig. 7, the NH_3-TPD and TG analyses have displayed that SO_4^{2-}/TiO_2(B) had obviously more acid amount than SO_4^{2-}/Anatase whereas they exhibited minor difference in sulfate group content. Simultaneously, Fig. 5 and Table 1 have also shown the higher percentage of Brønsted acid in SO_4^{2-}/TiO_2(B) compared with that in SO_4^{2-}/Anatase. Accordingly, it is deduced that SO_4^{2-}/TiO_2(B) has relatively higher ratio of bridged bidentate sulfate groups while SO_4^{2-}/Anatase possesses more chelating bidentate ones. Moreover, note that two Ti cations in each bridged bidentate coordinative acid site could together share responsibility for the electron donation, different from that only one electron donor exists in each acid site in chelating bidentate coordinative configuration. If the hypothesis were the case, the linked Ti cations in SO_4^{2-}/TiO_2(B) would show relatively weaker electron-deficient than those in SO_4^{2-}/Anatase. Thus, it needs to dissect the electronic structure of Ti element in solid superacids.

The XPS spectra of Ti2p and S2p of various samples are shown in Fig. 10. It can be seen that the Ti2p$_{3/2}$ and 2p$_{1/2}$ binding energies of both TiO_2(B) and Anatase are 458.3 eV and 464.0 eV, respectively, which are ascribed to the typical Ti^{4+} in titania [43]. In comparison, the Ti2p$_{3/2}$ and 2p$_{1/2}$ binding energies of SO_4^{2-}/TiO_2(B) and SO_4^{2-}/Anatase are shifted to higher values compared with their respective supports, suggesting the Ti cations in solid superacids are more electron deficient [64]. This demonstrates the formation of Lewis acid site in solid superacids [43].

Moreover, both SO_4^{2-}/TiO_2(B) and SO_4^{2-}/Anatase are confirmed to the existence of S^{6+} through the binding energy of fitted into two peaks ($S2p_{3/2}$ and $S2p_{1/2}$ doublet) at 168.8±0.1 eV and 170.0±0.1 eV [8, 65]. According to electron induction theory, only the hexavalent sulfur species could make solid superacid show superacidic property [2, 66]. It demonstrates the superacidity of SO_4^{2-}/TiO_2(B) and SO_4^{2-}/Anatase from electron structure analyses of elements. Correspondingly, NH_3-TPD results have proved the presence of strong acid sites in both SO_4^{2-}/TiO_2(B) and SO_4^{2-}/Anatase, as also demonstrated by they showing catalytic activity in alkylation reaction.

(Fig. 10)

On the other hand, noteworthy is that both SO_4^{2-}/TiO_2(B) and SO_4^{2-}/Anatase have a significantly different shift in binding energy of Ti cations compared with that of their respective supports. As shown in Fig. 10(a), the binding energy of $Ti2p_{3/2}$ in SO_4^{2-}/Anatase is 458.8 eV, which is 0.6 eV higher than that of Anatase. However, there is only 0.2 eV of binding energy shift between SO_4^{2-}/TiO_2(B) and TiO_2(B), obviously lower than that between SO_4^{2-}/Anatase and Anatase (0.2 eV versus 0.6 eV). This indicates the Ti cations of SO_4^{2-}/TiO_2(B) show relatively weaker electron-deficient than that of SO_4^{2-}/Anatase. This provides a strong evidence to the aforementioned inference about acid site structure of SO_4^{2-}/TiO_2(B) and SO_4^{2-}/Anatase. Moreover, the electron-deficiency of Ti cations corresponds to the acid strength of solid superacid [2, 43]. It means that the strength of bridged bidentate coordinative acid sites is weaker than that of chelating ones. This can account for the less amount of strong acid in SO_4^{2-}/TiO_2(B) compared with that in SO_4^{2-}/Anatase as listed in Table 1. Thus, it could be believed that there are more bridged

bidentate coordination of sulfate groups existed in $SO_4^{2-}/TiO_2(B)$ compared with those in $SO_4^{2-}/Anatase$.

Based on the results and discussion mentioned above, we can clarify the relationship between acid properties of $SO_4^{2-}/TiO_2(B)$ and acid site structure. As the structure model of acid site shown in Fig 9, one bridged bidentate sulfate group could induce two linked Ti cations to form Lewis acid site while one chelating bidentate sulfate group could induce to generate one acid site. With synergistic interaction of Lewis acid sites to neighboring water molecules, more Brønsted acid sites would be produced in the configuration of bridged bidentate coordination. Hence, under the same amount of sulfate group, more acid sites and higher ratio of Brønsted/Lewis acid sites could be formed in the configuration of bridged bidentate coordination compared with that in the chelating one. Furthermore, two electron donors are existed in each bridged bidentate acid site, varying from that only one Ti cation with chelating bidentate sulfate group could donate electron. Consequently, the Ti cations in bridged bidentate acid sites show relatively weak electron deficient, which further result in their weakened acid strength. As demonstrated above, more bridged bidentate coordination of sulfate groups existed in $SO_4^{2-}/TiO_2(B)$. Therefore, $SO_4^{2-}/TiO_2(B)$ possesses more total acid amount, higher percentage of Brønsted/Lewis acid sites but relatively weaker acid strength compared with that of $SO_4^{2-}/Anatase$.

Conclusions

In summary, the mesoporous $TiO_2(B)$ whisker-supported sulfated solid superacid was synthesized for the first time, and its acidic properties and the corresponding catalytic performance were systematically analyzed. Under the similar amount of sulfate group, $SO_4^{2-}/TiO_2(B)$ showed remarkably more acid amount, higher percentage of Brønsted acid, weaker acid strength compared with $SO_4^{2-}/Anatase$.

Different acid properties between $SO_4^{2-}/TiO_2(B)$ and $SO_4^{2-}/Anatase$ resulted in their varying catalytic performances of esterification and alkylation and catalytic selectivities. All of the experimental evidence were pointed to the formation of unique structural acid sites in $TiO_2(B)$. The structure-performance relationship analyses exhibited that the coordination of sulfate group with more Ti atoms of $TiO_2(B)$ was the key factor for influencing the formation of unique acid characteristics and further determining the corresponding catalytic results.

Acknowledgements

Notes and references

[1] H. Makoto, A. Kazushi, Chem. Lett., 8 (1979), 477-480. https://doi.org/10.1246/cl.1979.477

[2] K. Arata, Adv. Catal., 37 (1990), 165-211. https://doi.org/10.1016/S0360-0564(08)60365-X

[3] K. Arata, H. Matsuhashi, M. Hino, H. Nakamura, Catal. Today, 81 (2003), 17-30. https://doi.org/10.1016/S0920-5861(03)00098-1

[4] B. M. Reddy, M. K. Patil, Chem. Rev., 40 (2009), 2185. https://doi.org/10.1021/cr900008m

[5] K. Arata, Green Chem., 11 (2009), 1719-1728. https://doi.org/10.1039/B822795K

[6] F. Su, Y. Guo, Green Chem., 16 (2014), 2934-2957. https://doi.org/10.1039/C3GC42333F

[7] P. Gupta, S. Paul, Catal. Today, 236 (2014), 153-170. https://doi.org/10.1016/j.cattod.2014.04.010

[8] H. Zhao, P. Jiang, Y. Dong, M. Huang, B. Liu, New J. Chem., 38 (2014), 4541-4548. https://doi.org/10.1039/C4NJ00494A

[9] W. P. Shi, Catal. Lett., 143 (2013), 732-738. https://doi.org/10.1007/s10562-013-1016-4

[10] G. D. Yadav, N. P. Ajgaonkar, A. Varma, J. Catal., 292 (2012), 99-110. https://doi.org/10.1016/j.jcat.2012.05.004

[11] B. Chang, J. Fu, Y. Tian, X. Dong, Appl. Catal. A Gen., 437-438 (2012), 149-154. https://doi.org/10.1016/j.apcata.2012.06.031

[12] Y. M. Sani, W. M. A. W. Daud, A. R. Abdul Aziz, Appl. Catal. A Gen., 470 (2014), 140-161. https://doi.org/10.1016/j.apcata.2013.10.052

[13] Z. Miao, J. Zhou, J. Zhao, D. Liu, X. Bi, L. Chou, S. Zhuo, Appl. Suf. Sci., 411 (2017), 419-430. https://doi.org/10.1016/j.apsusc.2017.03.183

[14] A. Osatiashtiani, A. F. Lee, M. Granollers, D. R. Brown, L. Olivi, G. Morales, J. A. Melero, K. Wilson, ACS Catal., 5 (2015), 4345-4352. https://doi.org/10.1021/acscatal.5b00965

[15] J. B. Joo, A. Vu, Q. Zhang, M. Dahl, M. Gu, F. Zaera, Y. Yin, ChemSusChem, 6 (2013), 2001-2008. https://doi.org/10.1002/cssc.201300416

[16] G. Xiao, J. Zhou, X. Huang, X. Liao, B. Shi, RSC Adv., 4 (2014), 4010-4019. https://doi.org/10.1039/C3RA44083D

[17] Q. Shu, H. Yuan, B. Liu, L. Zhu, C. Zhang, J. Wang, Fuel, 143 (2015), 547-554. https://doi.org/10.1016/j.fuel.2014.11.081

[18] H. Yang, R. Lu, J. Zhao, X. Yang, L. Shen, Z. Wang, Mater. Chem. Phys., 80 (2003), 68-72. https://doi.org/10.1016/S0254-0584(02)00162-1

[19] T. Jin, T. Yamaguchi, K. Tanabe, J. Phys. Chem., 90 (1986), 4794-4796. https://doi.org/10.1021/j100411a017

[20] K. Parida, V. Quaschning, E. Lieske, E. Kemnitz, J. Mater. Chem., 11 (2001), 1903-1911. https://doi.org/10.1039/B009170G

[21] W. Stichert, F. Schüth, S. Kuba, H. Knözinger, J. Catal., 198 (2001), 277-285. https://doi.org/10.1006/jcat.2000.3151

[22] C. Morterra, G. Cerrato, F. Pinna, M. Signoretto, J. Catal., 157 (1995), 109-123. https://doi.org/10.1006/jcat.1995.1272

[23] N. A. Khan, D. K. Mishra, I. Ahmed, J. W. Yoon, J.-S. Hwang, S. H. Jhung, Appl. Catal. A Gen., 452 (2013), 34-38. https://doi.org/10.1016/j.apcata.2012.11.022

[24] H. Zhao, P. Jiang, Y. Dong, M. Huang, B. Liu, React. Kinet. Mech. Cat., 113 (2014), 445-458. https://doi.org/10.1007/s11144-014-0756-5

[25] X. Bokhimi, A. Morales, E. Ortíz, T. López, R. Gómez, J. Navarrete, J. Sol-Gel. Sci. Technol., 29 (2004), 31-40. https://doi.org/10.1023/B:JSST.0000016135.02238.0e

[26] R. Marchand, L. Brohan, M. Tournoux, Mater. Res. Bul., 15 (1980), 1129-1133. https://doi.org/10.1016/0025-5408(80)90076-8

[27] W. Li, C. Liu, Y. X. Zhou, Y. Bai, X. Feng, Z. H. Yang, L. H. Lu, X. H. Lu, K.-Y. Chan, J. Phys. Chem. C, 112 (2008), 20539-20545. https://doi.org/10.1021/jp808183q

[28] G. Wang, Q. Wang, W. Lu, J. Li, J. Phys. Chem. B, 110 (2006), 22029-22034. https://doi.org/10.1021/jp064630k

[29] Y. Ren, Z. Liu, F. Pourpoint, A. R. Armstrong, C. P. Grey, P. G. Bruce, Angew. Chem. Int. Edit., 124 (2012), 2206-2209. https://doi.org/10.1002/ange.201108300

[30] Y. Bai, W. Li, C. Liu, Z. H. Yang, X. Feng, X. H. Lu, K.-Y. Chan, J. Mater. Chem., 19 (2009), 7055-7061. https://doi.org/10.1039/B910240J

[31] W. J. Liu, J. G. Wang, W. Li, X. J. Guo, L. H. Lu, X. H. Lu, X. Feng, C. Liu, Z. H. Yang, Phys. Chem. Chem. Phys., 12 (2010), 8721-8727. https://doi.org/10.1039/B920128A

[32] W. Fang, W. J. Liu, X. J. Guo, X. H. Lu, L. H. Lu, J. Phys. Chem. C, 115 (2011), 8622–8629. https://doi.org/10.1021/jp110825y

[33] A. Vittadini, M. Casarin, A. Selloni, J. Phys. Chem. C, 113 (2009), 18973-18977. https://doi.org/10.1021/jp9073009

[34] W. Zhuang, L. H. Lu, X. B. Wu, W. Jin, M. Meng, Y. H. Zhu, X. H. Lu, Electronchem. Commun., 27 (2013), 124-127. https://doi.org/10.1016/j.elecom.2012.11.012

[35] M. He, X. H. Lu, X. Feng, L. Yu, Z. H. Yang, Chem. Commun., 10 (2004), 2202-2203. https://doi.org/10.1039/B408609K

[36] T. Beuvier, M. Richardplouet, L. Brohan, J. Phys. Chem. C, 113 (2009), 13703-13706. https://doi.org/10.1021/jp903755p

[37] B. Huang, C. H. Bartholomew, B. F. Woodfield, Micro. Meso. Mater., 184 (2014), 112-121. https://doi.org/10.1016/j.micromeso.2013.10.008

[38] J. R. Edison, P. A. Monson, Micro. Meso. Mater., 154 (2012), 7-15. https://doi.org/10.1016/j.micromeso.2011.12.029

[39] C. Meng, G. P. Cao, X. K. Li, Y. Z. Yan, E. Y. Zhao, L. Y. Hou, H. Y. Shi, React. Kinet. Mech. Cat., 121 (2017), 719-734. https://doi.org/10.1007/s11144-017-1165-3

[40] X. Hou, Y. Qiu, E. Yuan, X. Zhang, G. Liu, Appl. Catal. A Gen., 537 (2017), 12-23. https://doi.org/10.1016/j.apcata.2017.03.002

[41] F. Babou, G. Coudurie, J. C. Vedrine, J. Catal., 152 (1995), 341-349. https://doi.org/10.1006/jcat.1995.1088

[42] A. P. Kulkarni, D. S. Muggli, Appl. Catal. A Gen., 302 (2006), 274-282. https://doi.org/10.1016/j.apcata.2006.01.033

[43] F. Liu, T. Wang, Y. Zheng, J. Wang, J. Catal., 355 (2017), 17-25. https://doi.org/10.1016/j.jcat.2017.08.014

[44] C. A. Emeis, J. Catal., 141 (1993), 347-354. https://doi.org/10.1006/jcat.1993.1145

[45] Y. X. Jiang, X. M. Chen, Y. F. Mo, Z. F. Tong, J. Mol. Catal. A Chem., 213 (2004), 231-234. https://doi.org/10.1016/j.molcata.2003.12.014

[46] D. E. López, K. Suwannakarn, D. A. Bruce, J. G. Goodwin, J. Catal., 247 (2007), 43-50. https://doi.org/10.1016/j.jcat.2007.01.003

[47] Z. Li, R. Wnetrzak, W. Kwapinski, J. J. Leahy, ACS Appl. Mater. Interfaces, 4 (2012), 4499-4505. https://doi.org/10.1021/am300510u

[48] H. I. Ryoo, L. Y. Hong, S. H. Jung, D.-P. Kim, J. Mater. Chem., 20 (2010), 6419-6421. https://doi.org/10.1039/C0JM01174F

[49] X. Sun, Q. Wang, L. Xu, S. Liu, Catal. Lett., 94 (2004), 75-79. https://doi.org/10.1023/B:CATL.0000019334.10713.63

[50] C. Tagusagawa, A. Takagaki, S. Hayashi, K. Domen, Catal. Today,

142 (2009), 267-271. https://doi.org/10.1016/j.cattod.2008.10.045

[51] M. A. Harmer, W. E. Farneth, Q. Sun, J. Am. Chem. Soc., 118 (1996), 7708-7715. https://doi.org/10.1021/ja9541950

[52] C. Tagusagawa, A. Takagaki, A. Iguchi, K. Takanabe, J. N. Kondo, K. Ebitani, S. Hayashi, T. Tatsumi, K. Domen, Angew. Chem. Int. Edit., 122 (2010), 1146-1150. https://doi.org/10.1002/anie.200904791

[53] C. Ramesh Kumar, N. Rambabu, K. C. Maheria, A. K. Dalai, N. Lingaiah, Appl. Catal. A Gen., 485 (2014), 74-83. https://doi.org/10.1016/j.apcata.2014.07.034

[54] L. K. Noda, N. S. Gonçalves, S. M. D. Borba, J. A. Silveira, Vib. Spectrosc., 44 (2007), 101-107. https://doi.org/10.1016/j.vibspec.2006.09.009

[55] J. Gardy, A. Hassanpour, X. Lai, M. H. Ahmed, Appl. Catal. A Gen., 527 (2016), 81-95. https://doi.org/10.1016/j.apcata.2016.08.031

[56] M. Hino, M. Kurashige, H. Matsuhashi, K. Arata, Thermochim. Acta, 441 (2006), 35-41. https://doi.org/10.1016/j.tca.2005.11.042

[57] R. Srinivasan, R. A. Keogh, D. R. Milburn, B. H. Davis, J. Catal., 153 (1995), 123-130. https://doi.org/10.1006/jcat.1995.1114

[58] A. Desmartin-Chomel, J. L. Flores, A. Bourane, J. M. Clacens, F. Figueras, G. Delahay, A. G. Fendler, C. Lehaut-Burnouf, J. Phys. Chem. B, 110 (2006), 858-863. https://doi.org/10.1021/jp0530698

[59] G. X. Yan, A. Q. Wang, I. E. Wachs, J. Baltrusaitis, Appl. Catal. A Gen., (2019), in press. https://doi.org/10.1016/j.apcata.2018.12.012

[60] Y. Hu, B. Guo, Y. Fu, Y. Ren, G. Tang, X. Chen, B. Yue, H. He, Chem. Commun., 51 (2015), 14219. https://doi.org/10.1039/C5CC04548G

[61] X. H. Lin, S. F. Y. Li, Appl. Catal. B Environ., 170-171 (2015), 263-272. https://doi.org/10.1016/j.apcatb.2015.02.001

[62] J. L. Ropero-Vega, A. Aldana-Pérez, R. Gómez, M. E. Niño-Gómez, Appl. Catal. A Gen., 379 (2010), 24-29. https://doi.org/10.1016/j.apcata.2010.02.020

[63] F. Haase, J. Sauer, J. Am. Chem. Soc., 120 (1998), 13503-13512. https://doi.org/10.1021/ja9825534

[64] X. Fu, W. A. Zeltner, Q. Yang, M. A. Anderson, J. Catal., 168 (1997), 482-490. https://doi.org/10.1006/jcat.1997.1660

[65] E. J. Romano, K. H. Schulz, Appl. Suf. Sci., 246 (2005), 262-270. https://doi.org/10.1016/j.apsusc.2004.11.017

[66] R. S. Drago, N. Kob, J. Phys. Chem. B, 101 (1997), 3360-3364. https://doi.org/10.1021/jp962515b

List of Figure captions

Fig. 1 Raman spectra of $SO_4^{2-}/TiO_2(B)$ and $SO_4^{2-}/Anatase$
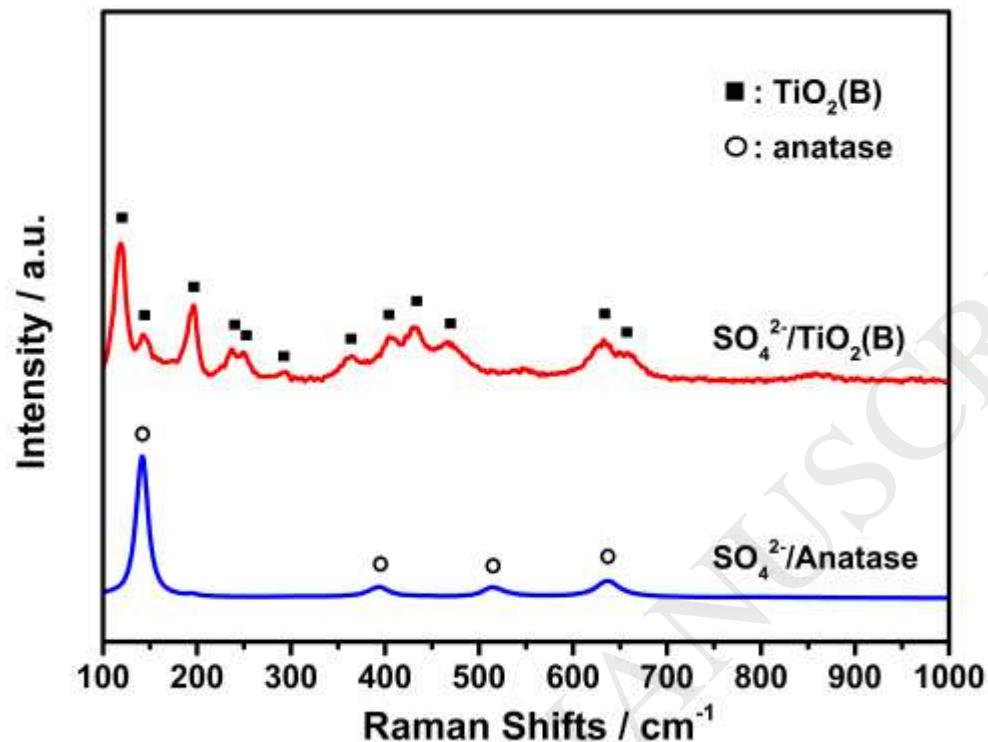
Fig. 2 SEM images (a, b), low resolution (c, d) and high resolution (e, f) TEM images of $SO_4^{2-}/TiO_2(B)$ and $SO_4^{2-}/Anatase$
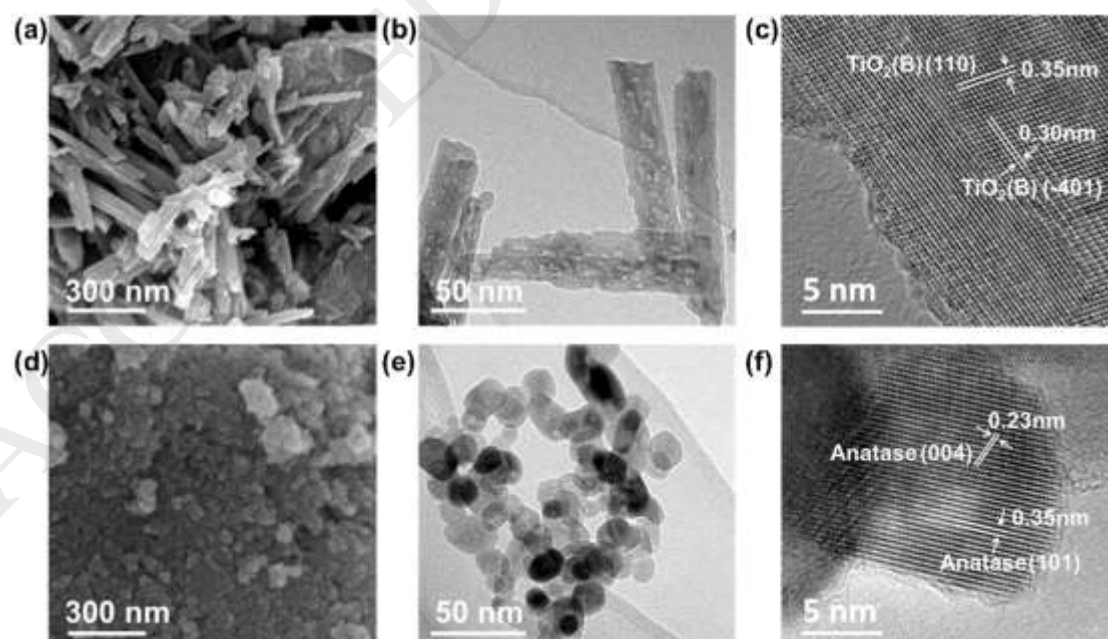
Fig. 3 Nitrogen adsorption-desorption isotherms and pore size distribution of $SO_4^{2-}/TiO_2(B)$ and $SO_4^{2-}/Anatase$
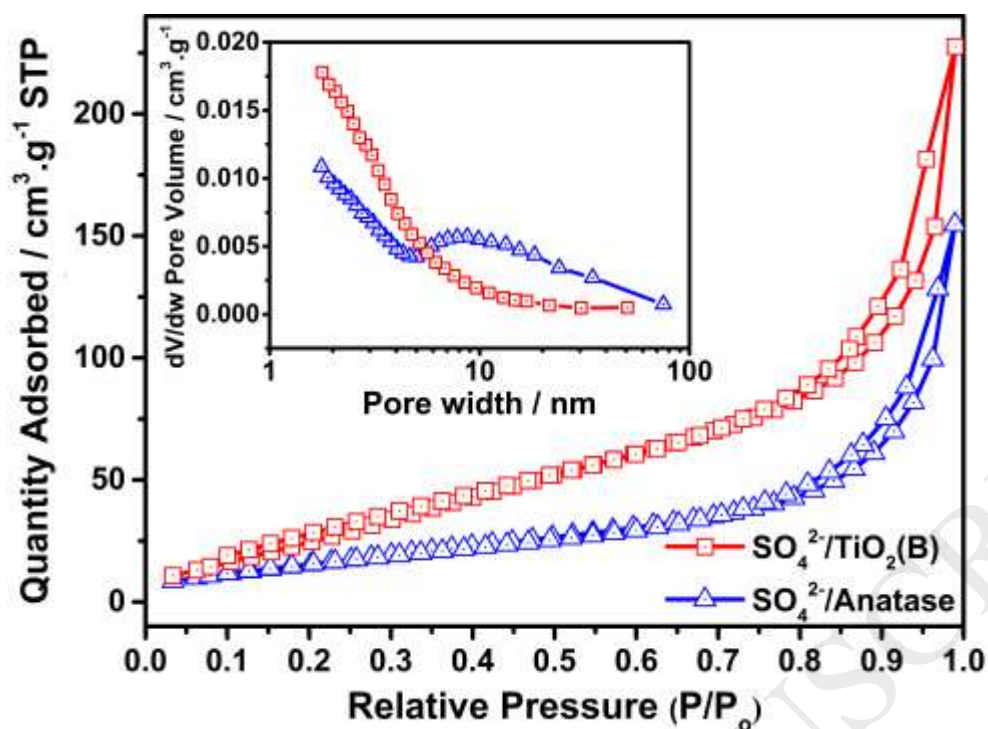
Fig. 4 NH$_3$-TPD profiles of SO$_4^{2-}$/TiO$_2$(B) and SO$_4^{2-}$/Anatase
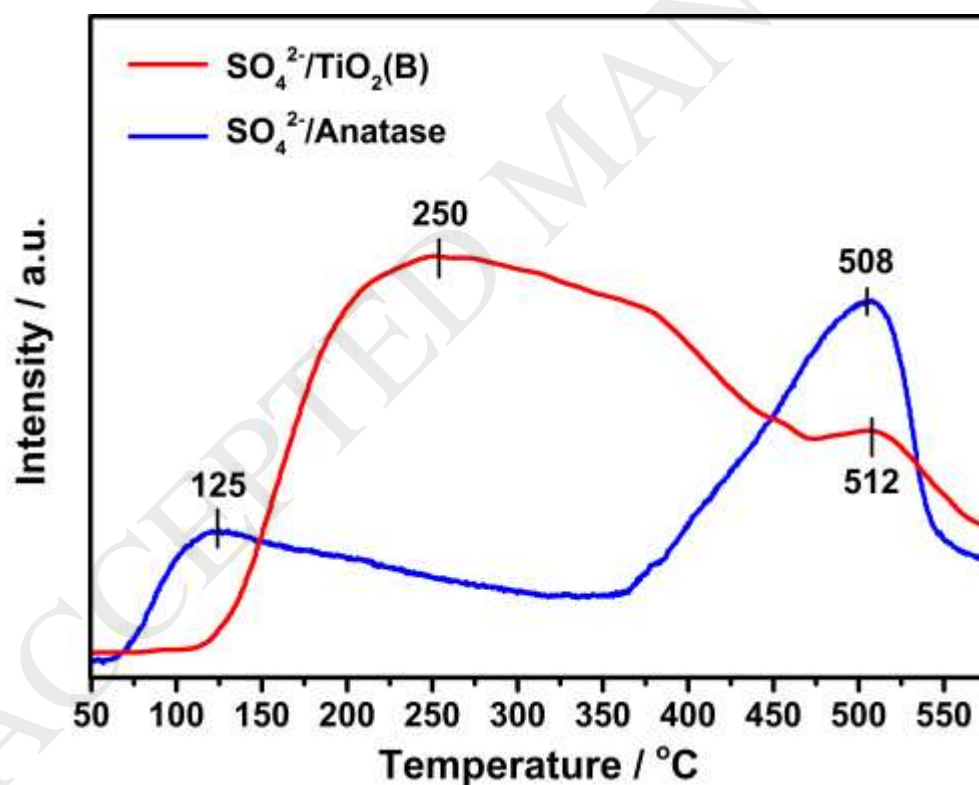
Fig. 5 Py-IR spectra of SO$_4^{2-}$/TiO$_2$(B), SO$_4^{2-}$/Anatase and their corresponding supports
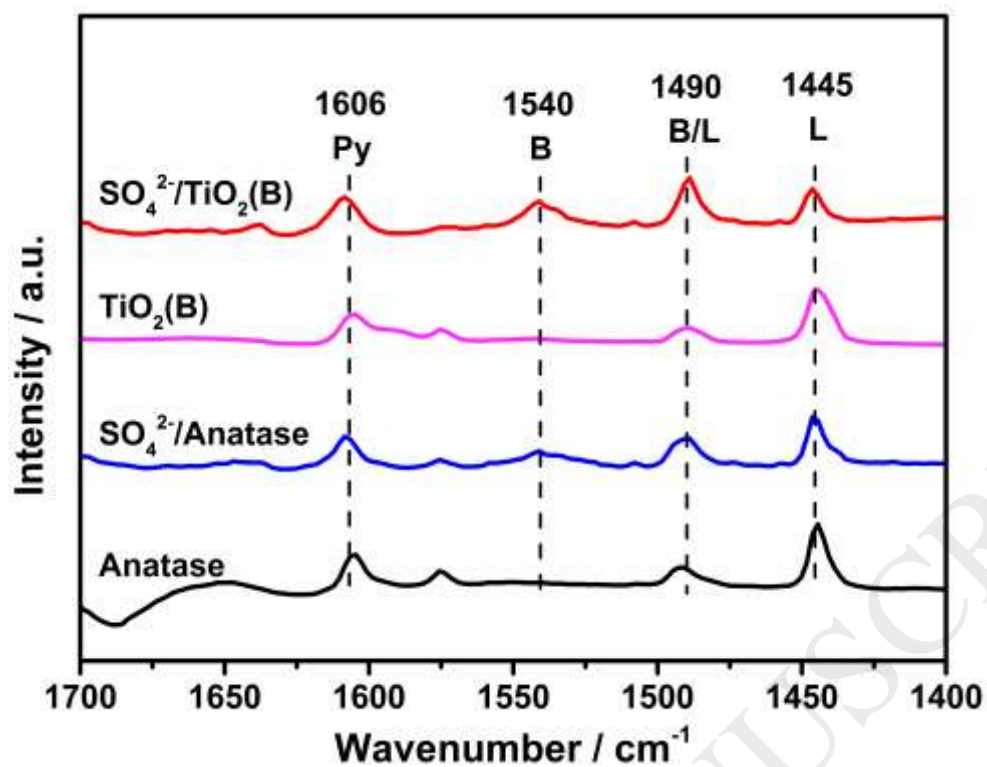
Fig. 6 Natural settling process of (a) $SO_4^{2-}/TiO_2(B)$ and (b) $SO_4^{2-}/Anatase$ in suspensions and their cycling results
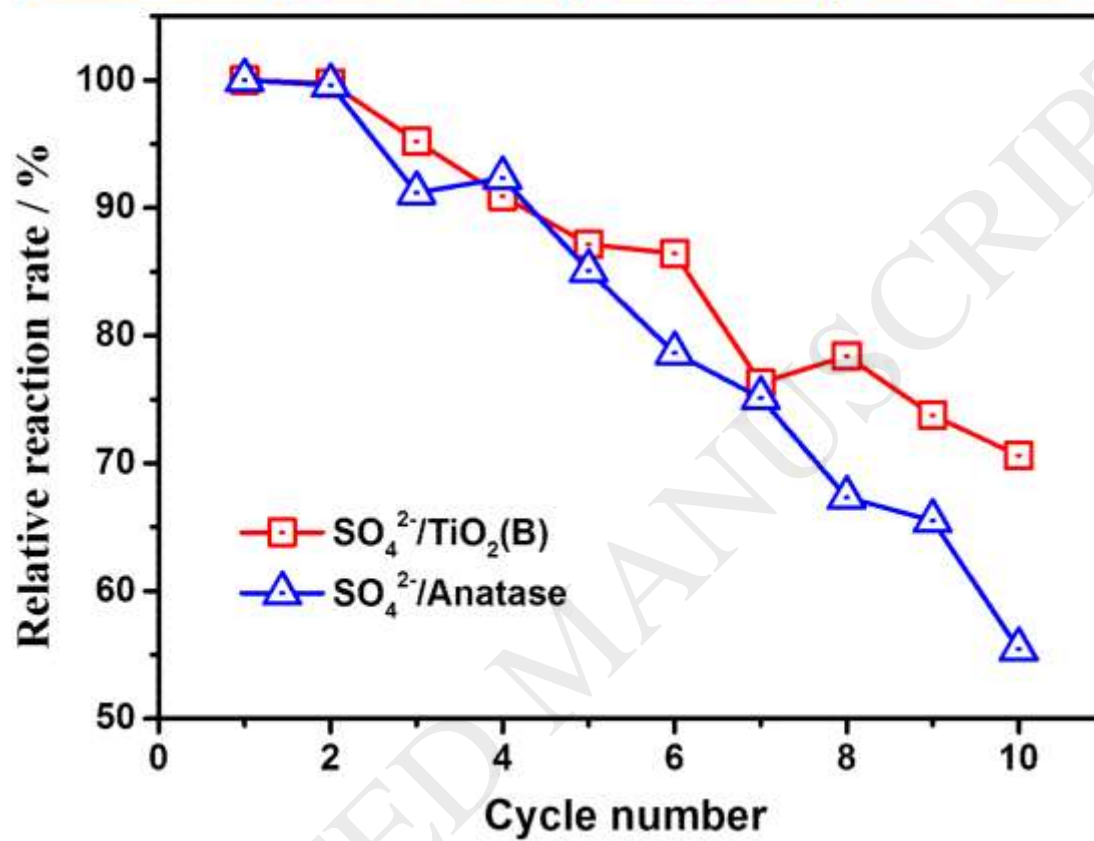
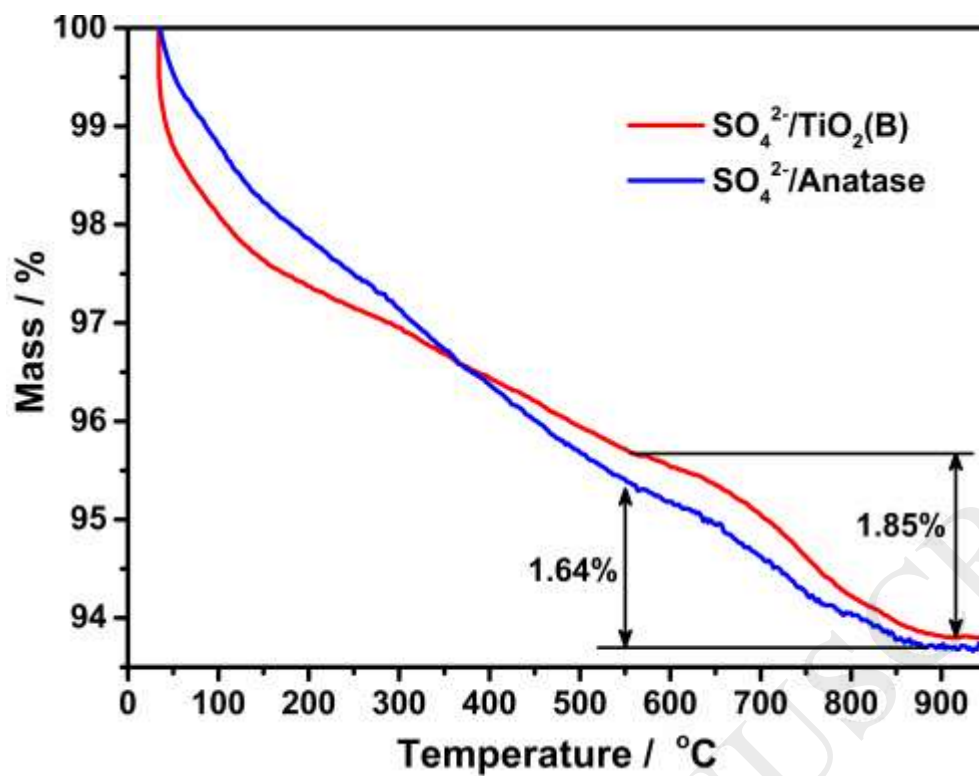**Fig. 7**   TG patterns of $SO_4^{2-}/TiO_2(B)$ and $SO_4^{2-}/Anatase$

Fig. 8 FT-IR spectra of $SO_4^{2-}/TiO_2(B)$ and $SO_4^{2-}/Anatase$
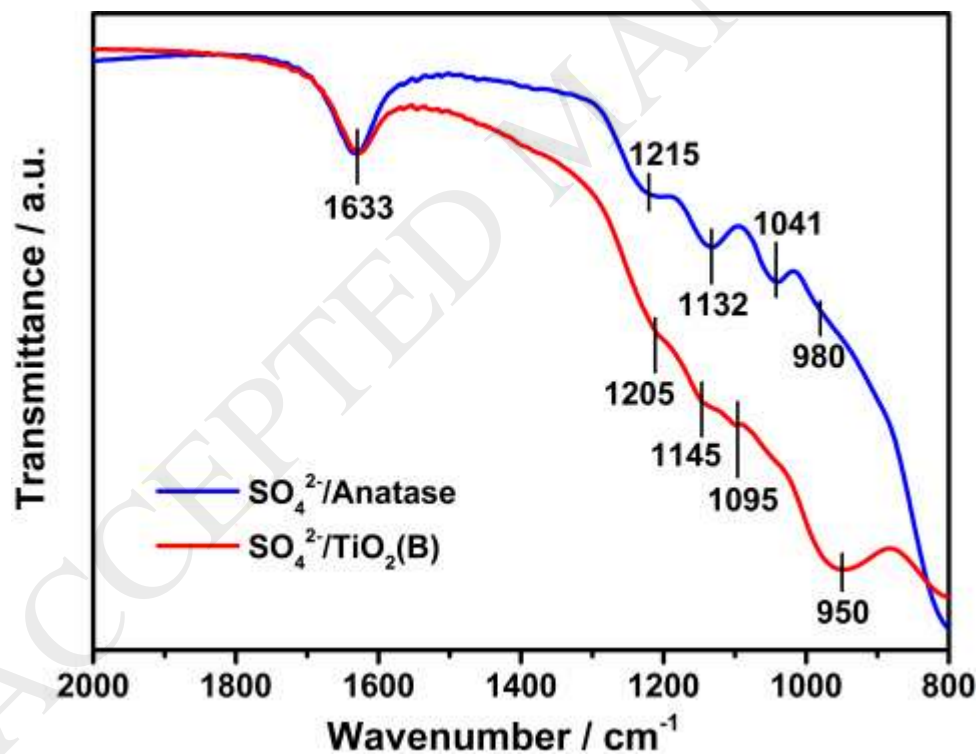
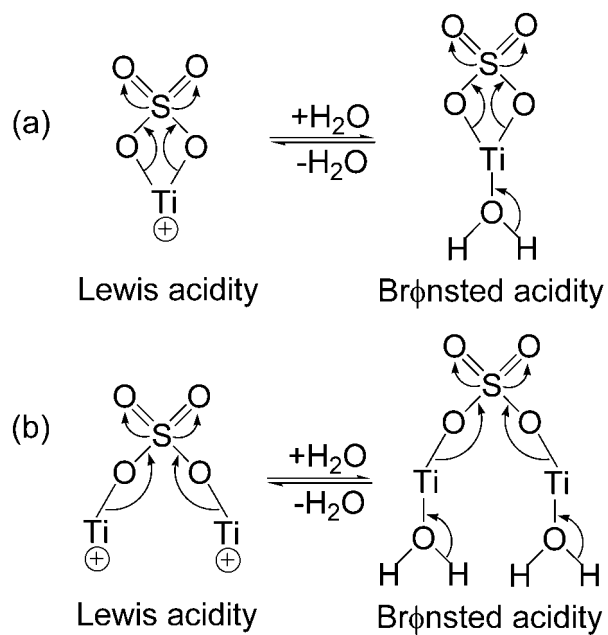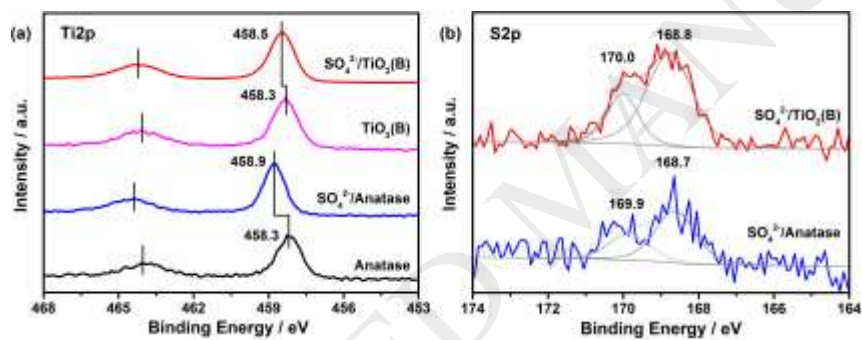**Fig. 9** Scheme for the structure of Lewis and Brønsted acid sites in $SO_4^{2-}/TiO_2(B)$ and $SO_4^{2-}/Anatase$

(a)

Lewis acidity   Brφnsted acidity

(b)

Lewis acidity   Brφnsted acidity

Fig. 10 (a) Ti2p and (b) S2p XPS spectra of various samples

List of Table

Table 1 Physicochemical properties of $SO_4^{2-}/TiO_2(B)$ and $SO_4^{2-}/Anatase$

Samples	Structural properties			Acid amount and strength distribution[α]				Acid type	
	S_{BET} $(m^2 \cdot g^{-1})$	V_p $(cm^3 \cdot g^{-1})$	$W_{SO_4^{2-}}$ (wt%)	N_{Total} $(\mu mol \cdot g^{-1})$	N_{Weak} $(\mu mol \cdot g^{-1})$	N_{Medium} $(\mu mol \cdot g^{-1})$	N_{Strong} $(\mu mol \cdot g^{-1})$	$X_{Brønsted}$ (mol%)	X_{Lewis} (mol%)
$SO_4^{2-}/TiO_2(B)$	78.8	0.10	2.22	33.3	3.9	22.8	6.6	70.9	29.1
$SO_4^{2-}/Anatase$	63.1	0.24	1.97	18.8	3.6	6.9	8.3	41.5	58.5

α: acid amount is measured by molar amount of adsorbed NH_3 molecules per unit mass of solid superacid.

Table 2 The reaction rate and selectivity results of various solid superacids

Samples	Esterification	Alkylation			
	r_E $(mmol_{BuOH} \cdot g^{-1} \cdot min^{-1})$	r_A $(mmol_{BA} \cdot g^{-1} \cdot min^{-1})$	S_{Ortho} (%)	S_{Para} (%)	$S_{Dibenzylether}$ (%)
$SO_4^{2-}/TiO_2(B)$	4.25	1.39	26.05	53.37	20.57
$TiO_2(B)$	1.15	0	/	/	/
$SO_4^{2-}/Anatase$	2.87	1.95	24.60	49.31	26.07
Anatase	0.95	0	/	/	/